Impact of the Use of Sterically Congested Cyclometalated Ligands on the Optoelectronic Properties and Device Performances In Light-Emitting Electrochemical Cells of Cationic Iridium(III) Complexes

Claus Hierlinger,[a,b] *Elzbieta Trzop,*[c] *Loïc Toupet,*[c] *Jorge Ávila,*[d] *Henk J. Bolink,*[d] *Véronique Guerchais**[a] *Eli Zysman-Colman**[b]

[a] Univ Rennes, CNRS, ISCR (Institut des Sciences Chimiques de Rennes) – UMR 6226, F-35000 Rennes, France. E-mail: veronique.guerchais@univ-rennes1.fr

[b] Organic Semiconductor Centre, EaStCHEM School of Chemistry, University of St Andrews, St Andrews, Fife, KY16 9ST, UK. E-mail: eli.zysman-colman@st-andrews.ac.uk; Web: http://www.zysman-colman.com

[c] Univ Rennes, CNRS, IPR (Institut de Physique de Rennes) - UMR 6251, F-35000 Rennes, France

[c] Instituto de Ciencia Molecular, Universidad de Valencia, C/J. Beltran 2, 46980 Paterna, Spain

Abstract

The synthesis, structural and optoelectronic characterization of a family of sterically congested cyclometalated cationic Ir(III) complexes of the form $[Ir(C^N)_2(d\textit{t}Bubpy)]PF_6$ (with d*t*Bubpy

= 4,4′-di-*tert*-butyl-2,2′-bipyridine and C^N = a cyclometalating ligand decorated at the 4-position of the pyridine ring and/or the 3-position of the phenyl ring with a range of sterically bulky substituents) are reported. This family of complexes is compared to the unsubstituted analogue complex **R1** bearing 2-phenylpyridinato as cyclometalating ligand. The impact of the use the sterics on the C^N ligands on both the solid state photophysics and light-emitting electrochemical cell (LEEC) device performance is investigated. X-ray diffraction analysis of complexes **1a, R2**, **2a**, and **1b** show an increasing internuclear distance in the solid state, within these four complexes. Emission studies in solution and neat film show that the chosen substituents essentially do not impact the emission energy. The photoluminescence quantum yields (Φ_{PL}) are in the same range (Φ_{PL} ~ 25 – 31%), except for **1b**, which shows a lower Φ_{PL} of 12%. All complexes exhibit similar monoexponential emission lifetimes in the submicrosecond regime. LEECs based on **R1, 1a, 1b** and **R2** were fabricated, showing yellow luminescence and moderate efficiencies and lifetimes. The arguably best performing LEEC device, showing the highest luminance (737 cd m^{-2}), current efficiency (7.4 cd A^{-1}) and EQE (2.6%), employed emitter **1a**.

Introduction

Iridium(III) complexes have a remarkable combination of photophysical properties,[1] including high photoluminescence quantum yields, Φ_{PL}, wide colour tenability, relatively short-lived phosphorescence lifetimes, τ_{PL}, that make them the go-to emitter class in solid-state electroluminescence (EL) devices, such as organic light emitting diodes (OLEDs)[2] and in light emitting electrochemical cells (LEECs).[3] LEECs possess a much simpler design, with fewer layers, compared to OLEDs,[4] as they typically employ an ionic emissive material that is dually responsible for charge mobility and the emission of light within the device. The most popular

and widely studied class of emitters for LEECs is the heteroleptic cationic Ir(III) complex of the form $[Ir(C^N)_2(N^N)]PF_6$ (C^N is a cyclometalating ligand, N^N is a diimine ancillary ligand).

Unlike in OLEDs where the emissive compound is present in only small concentrations as a dopant within a higher bandgap host, in LEECs the emissive layer is frequently composed either of a homogenous layer of emitter molecules or the emitter is the major component within the layer. As a consequence, one issue that can limit device performance is excited state self-quenching during device operation.[5] A strategy to circumvent this issue is to decorate the complexes with bulky, hydrophobic substituents that serve to increase the intermolecular distance while simultaneously hindering the disadvantageous attack of small molecules.[6] Chart **1** shows representative literature examples of iridium complexes (**R1-R9**) bearing bulky substituents that have been used as emitters in light-emitting electrochemical cells.

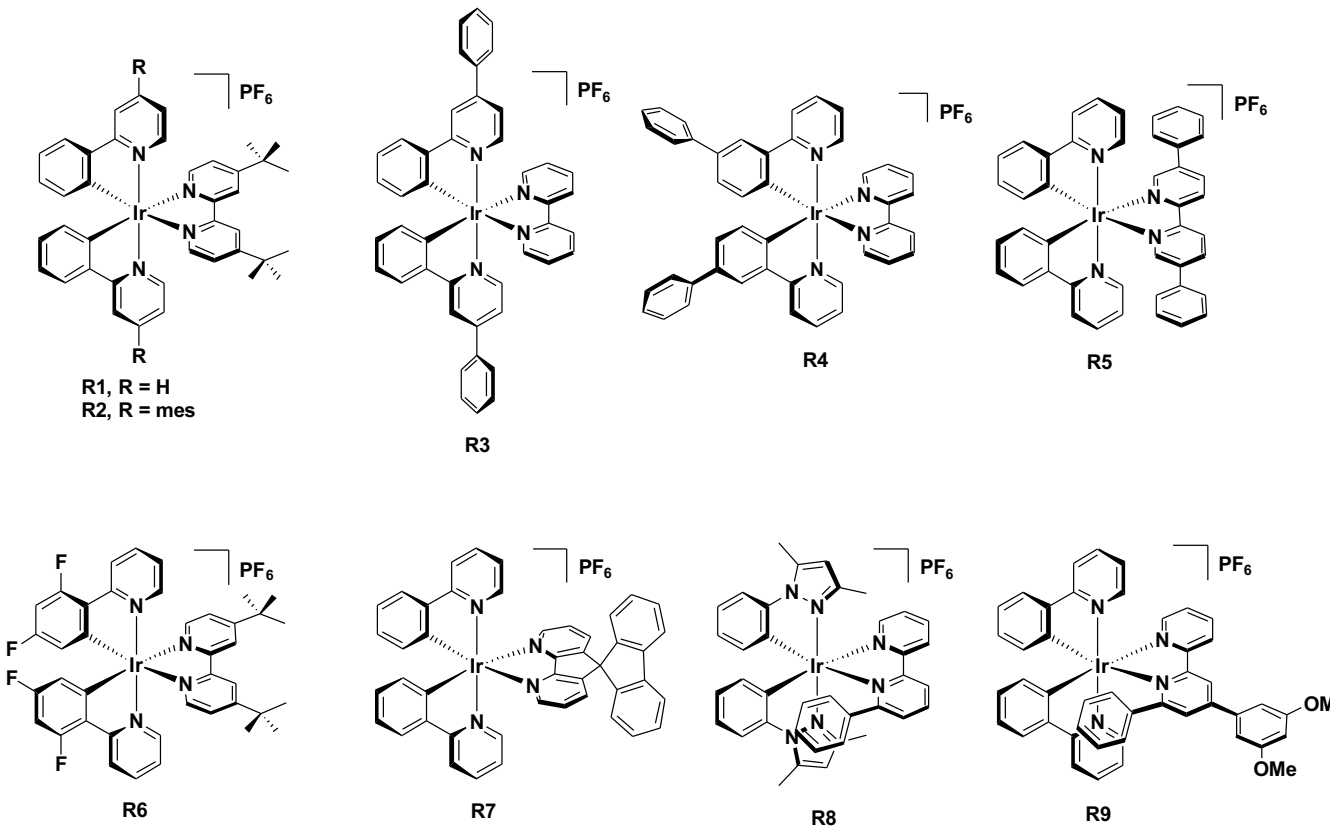

Chart **1**. Representative literature examples of iridium complexes bearing bulky substituents.

A successful molecular design that was applied to charge-neutral Ir(III) complexes for OLEDs was the incorporation of mesityl substituents at the C(4) position of the pyridyl ring of the ppy ligands in [Ir(dFmesppy)$_2$(pic)] (dFmesppyH = 2-(4,6-Difluorophenyl)-4-(mesityl)-pyridine and pic = picolinate). An increase in the photoluminescence quantum yield, Φ_{PL}, was observed, which also translated into enhanced external quantum efficiencies of the OLED devices compared to that employing the well-known [Ir(dFppy)$_2$(pic)], FIrpic (dFppyH = 2-(4,6-difluorophenyl)pyridine).[7] The enhancement in EQE compared to the FIrpic-based devices was attributed to reduced concentration quenching and increased solubility in organic solvents and therefore better dispersion during the fabrication of the solution-processed device. Notably, the mesityl group adopts an orthogonal conformation relative to the pyridine ring, resulting in

a disruption of the conjugation between these two aryl groups, minimizing the impact on the emission energy. Such an approach has been applied to cationic iridium complexes by us, where we have observed an enhancement of solution- and solid-state Φ_{PL} compared to the non-decorated analog complex.[8]

A comparison of **R1** and **R2** of the form $[Ir(C^N)_2(d\textit{t}Bubpy)]PF_6$ (where C^N is ppy or mesppy for **R1** and **R2**, respectively and d*t*Bubpy is 4,4′-di-*tert*-butyl-2,2′-bipyridine) reveals the impact of the mesityl group on the photophysical properties in cationic complexes.[8a] In CH_2Cl_2, the same emission maximum (λ_{PL} = 577 nm) is observed for both complexes while the Φ_{PL} is moderately enhanced for the mesitylated complex (Φ_{PL} = 35 and 40% for **R1** and **R2**, respectively). The LEECs fabricated with **R1**,[8a] showed a lifetime of $t_{1/2}$ = >1300 h and an EQE of 2.5%. Surprisingly and in contrast to the above-mentioned impact of the mesityl group, for LEECs based on **R2** there was a reduction in the device lifetime ($t_{1/2}$ = 0.6 h) and EQE (1.4%) upon incorporation of the mesityl groups on the C^N ligands. However, with **R2** faster response times could be achieved in devices compared to those based on **R1**, as the mesityl groups induce a more efficient electronic communication and recombination within the device, which results in faster turn-on times. The related complex $[Ir(dPhPy)_2(bpy)]PF_6$, **R3** (where dPhPy is 2,4-diphenylpyridine and bpy is 2,2′-bipyridine) bears a phenyl group on the 4-position of the pyridine of the C^N ligand in lieu of a mesityl group and contains a bpy N^N ligand in lieu of the d*t*Bubpy ligand.[9] In CH_2Cl_2, complex **R3** exhibits yellow phosphorescence (λ_{em} = 598 nm) with a Φ_{PL} of 21% . A single-layer LEEC based on **R3** containing a lithium salt additive showed improved device performance compared to the unsubstituted analogue. The device with **R3** displayed a short response time (t_{on} = 5 min), favorable lifetime (extrapolated lifetime calculated at 100 cd m^{-2}, $t_{1/2}L_{100}$ of 3800 h), and a peak luminance of 5500 cd m^{-2} (with t_{on} = 191 min, $t_{1/2}L_{100}$ = 4752 h and a peak luminance of 2753 cd m^{-2} for the unsubstituted analog). The authors

ascribed the improved LEEC performance to the bulky, hydrophobic nature of the phenyl substituent, which they asserted impeded self-quenching pathways of the Ir(III) complex. Another analogous complex is $[Ir(Phppy)_2(bpy)]PF_6$, **R4** (where Phppy is 2-([1,1'-biphenyl]-3-yl)pyridine), bearing a phenyl group *trans* to the Ir-C_{C^N} bond. Complex **R4** exhibits a yellow-orange emission with a Φ_{PL} of 13% in CH_2Cl_2. LEECs based on **R4** are likewise highly stable with $t_{1/2}$ = 2800 h and also are very bright with a maximum luminance of 1024 cd m^{-2}.[10]

The use of the sterically congested the d*t*Bubpy in **R6**[11] coupled with dFppy ligands contributed to a record maximum external quantum efficiency in the LEEC of 15%,[11a] significantly higher than that reported for the LEECs with **R1**, with EQE values ranging from 0.6 - 5.0%.[8a, 12] LEECs fabricated with **R5**[12b] incorporating a bulky ancillary ligand (5,5´-diphenyl-2,2´-bipyridine, dpbpy) showed long device lifetimes of 110 h (LEEC operating at 4 V), particularly compared to $[Ir(ppy)_2(dtBubpy)]PF_6$, **R1** (1.3 h). Using **R7**,[5] which contained the 4,5-diaza-9,9´-spirobifluorene ancillary ligand, resulted in LEECs with a maximum external quantum efficiencies of 7.1% at a device lifetimes of 12 h and luminance value of 52 cd m^{-2}.

Very stable LEECs have been fabricated employing emissive complexes where there is a phenyl ring positioned adjacent to one of the coordinating nitrogen atoms of the ancillary ligand as exemplified in $[Ir(dmppz)_2(pbpy)]PF_6$, **R8**, (where dmppz is 3,5-dimethyl-1-phenylpyrazole and pbpy is 6-phenyl-2,2´-bipyridine).[13] The phenyl ring of the pbpy forms a face-to-face π-stacking with the pyrazole unit of the C^N ligand, which insulates the complex from adventitious attack from small molecules.[14] High stability LEECs were fabricated with the complex $[Ir(ppy)_2(Meppbpy)]PF_6$, **R9**, (where Meppbpy is 4-(3,5-dimethoxyphenyl)-6-phenyl-2,2'-bipyridine) with a device lifetime of over 950 h and high luminance and current efficiency

(183 cd m^{-2} and 8.2 cd A^{-1}, respectively).[15] In the majority of cases, decorating the complex with bulky, hydrophobic substituents greatly improves the stability of LEECs.

These previous findings prompted us to design a family of cationic Ir(III) complexes of the form $[Ir(C^N)_2(dtBubpy)]PF_6$ in which the sterics about the C^N ligands are systematically modified via a combination of decoration at the 4-position of the pyridine ring and/or the 3-position of the phenyl ring in order to ascertain how the steric requirements affect the photophysics of the complexes and the corresponding LEEC device performance (Figure **1**). Complexes **R1** and **R2** were included into this study to serve as references.

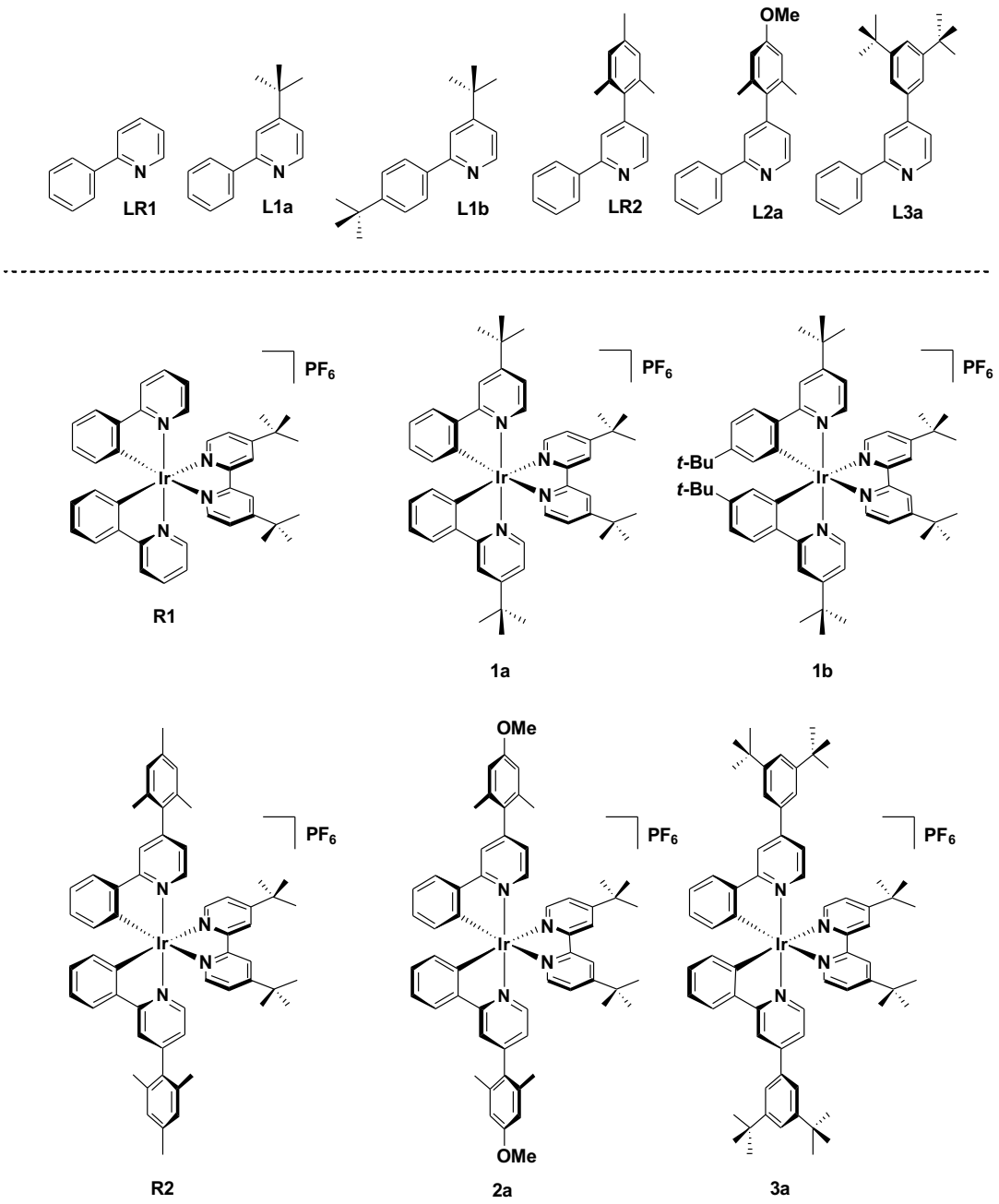

Figure **1**. Proligands and Ir(III) complexes under investigation in this study.

Results and Discussion

Synthesis of the C^N ligands

The family of substituted 2-phenylpyridine (ppyH) cyclometalating C^N ligands bearing R_1 (at the 4-pyridine position) and R_2 (at the 4-phenyl position) can be divided into two classes: 4-

substituted 2-phenylpyridine derivatives **L1a, LR1, L2a** and **L3a** [with R_1 = *tert*-butyl (*t*Bu), mesityl (mes), manisyl (man) – 4-methoxy-2,6-dimethylphenyl, and 3,5-di-*tert*-butylphenyl (d*t*Buphen), respectively, and R_2 = H]**,** and the substituted arylpyridine **L1b** (where R_1 = R_2 = *tert*-butyl). The ligand **LR1** is the unsubstituted ppyH (Figure **1**).

Compounds **L1a** and **L1b** are accessible as colourless oils from 4-*tert*-butylpyridine *via* a Minisci reaction[16] in moderate yields (45 and 46%, respectively), while **LR1** was commercially available. For **LR2, L2a** and **L3a**, a two-step Suzuki-Miyaura cross-coupling strategy was adapted from 2-chloro-4-iodopyridine (Scheme **1**).[8c] The mono-arylated 2-chloro-4-substituted compounds **ClR2, Cl2a** and **Cl3a** were isolated in excellent yields (94-96%) after purification by column chromatography. Key to the high yields is the use of excess $R_1B(OH)_2$, which led to easier purification of the intermediate 4-aryl-2-chloropyridines. A second Suzuki-Miyaura reaction with $PhB(OH)_2$ afforded **LR1, L2a** and **L3a** in excellent yields (86-90%) (Scheme **1**).

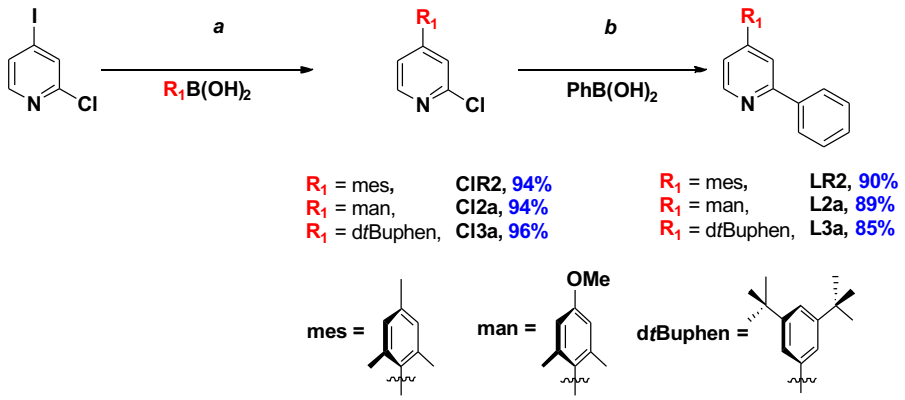

Scheme **1.** Synthesis scheme for compounds **LR1, L2a** and **L3a** (with R_1 = mes, man and d*t*Bphen, respectively). [a] $R_1B(OH)_2$, K_2CO_3, $Pd(PPh_3)_4$, dioxane/H_2O (4/1), 95 °C, 3 d; [b] $PhB(OH)_2$, K_2CO_3, $Pd(PPh_3)_4$, dioxane/H_2O (4/1), 95 °C, 18 h.

Synthesis of the Ir(III) complexes

The target complexes were synthesised *via* a two-step literature procedure (Scheme **2**). The C^N ligands were each first reacted with $IrCl_3{\cdot}6H_2O$ to afford the corresponding $[Ir(C^N)_2Cl]_2$ dimers in excellent yields (79-89%).[17] These intermediate dimers were then reacted with d*t*Bubpy in the presence of $AgPF_6$ to afford the desired heteroleptic complexes as yellow solids in generally excellent yields (79-92%) as their hexafluorophosphate salts.[18] Through the systematic increase of steric bulk of the cyclometalated ligands, the corresponding $[Ir(C^N)_2Cl]_2$ dimers as well as the cationic complexes show increased solubility in organic solvents such as CH_2Cl_2, $CHCl_3$ and MeCN compared to $[Ir(ppy)_2Cl]_2$ and the reference complex **R1**. Recrystallization from pentane/diethyl ether gave pure **R1**, whereas for the other complexes (**1a, 1b, R2, 2a** and **3a**) column chromatography on silica (eluent: 5% MeOH in CH_2Cl_2) was required. Following chromatographic purification, a second anion exchange reaction with NH_4PF_6 was conducted to ensure that the sole counterion was PF_6^-.

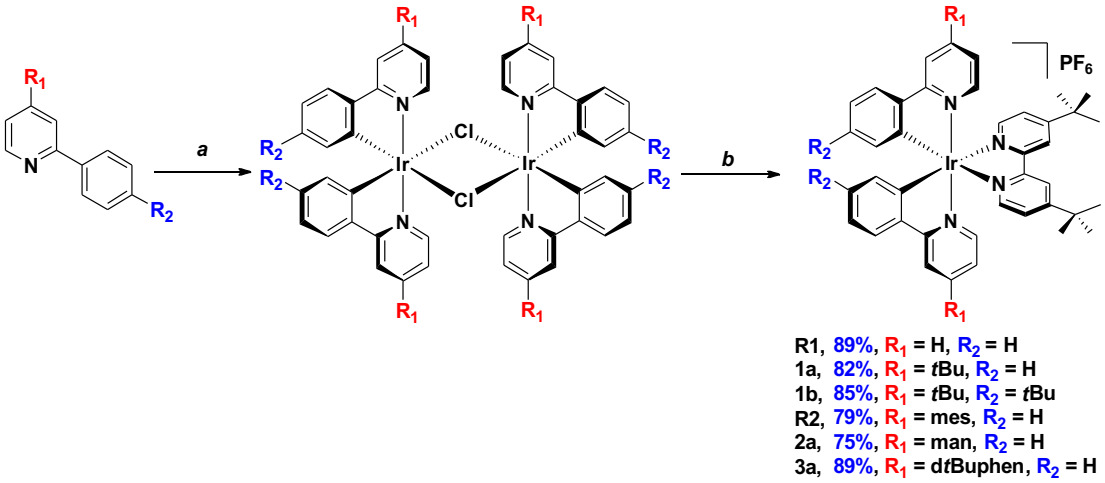

Scheme **2**. Synthesis of target complexes. [a] $IrCl_3.6H_2O$, 2-ethoxtyethanol/H_2O (3/1), 125 °C, 24 h. [b] 1) 4,4'-di-*tert*-butyl-2,2'-bipyridine, $AgPF_6$, 1,2-dichloroethane, 85 °C, 2h. 2) r.t., 12h.

X-ray structural studies

Single crystals of sufficient quality of **1a, 1b, R2** and **2a** were grown from CH_2Cl_2/Et_2O. The determined space groups are $P\bar{1}$ (for **1a**) and $P2_1$ (for **1b, R2** and **2a**). The crystal structure of **R2** has been previously reported; however, in the previous report the crystallization conditions were different.[8a] The crystal structure of **1a**, **1b**, **R2** and **2a** are presented in Figure **2**.

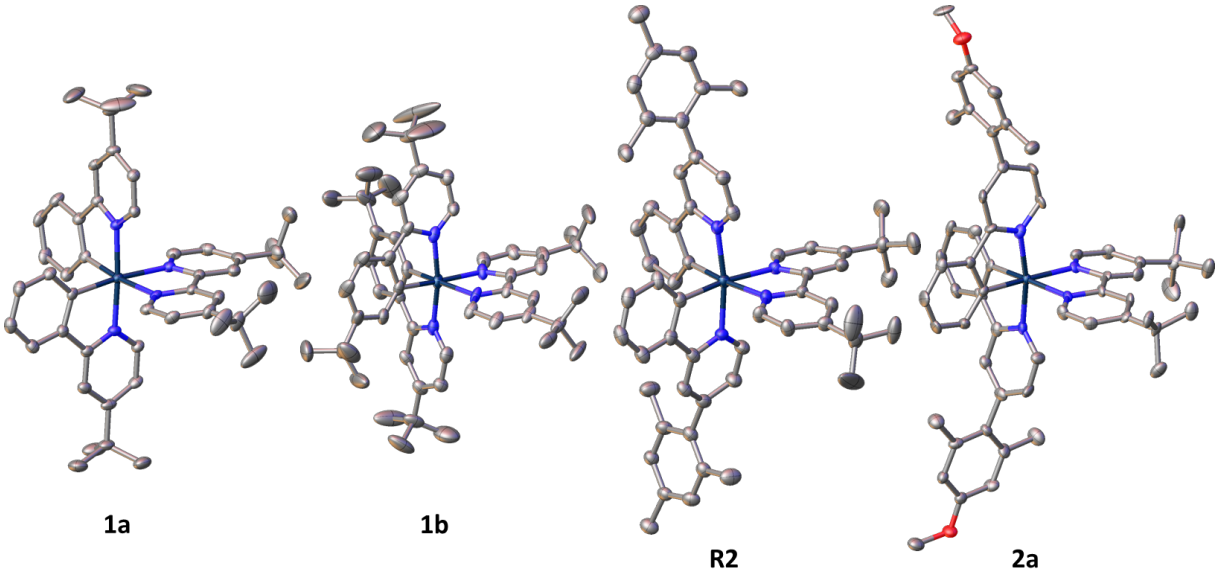

Figure **2.** Representation of the crystal structure of **1a, 1b, R2** and **2a**. The hydrogen atoms, solvent molecules, minor disorder, as well as the counter ion PF_6^- are omitted for clarity.

All complexes show the expected distorted octahedral geometry around the Ir centre with the pyridyl units of the C^N ligands mutually *trans* to each other, as is commonly seen in other cationic Ir(III) complexes of the form $[Ir(C^N)_2(N^N)]PF_6$.[1c, 19] The bond lengths and bond angles are as expected for this class of iridium complex. The torsion angles based on the angle between the planes of the R_1 aryl and the pyridine rings of the two C^N ligands in **R2** are 78.32° and 88.70° and in **2a** are 81.58° and 89.97°, which are similar to those previously reported for arylated C^N ligands in charged complexes,[8b-d] but are notably larger to those

found in **R3** for which an average torsion angle of 26° between the phenyl and the pyridine rings of the C^N ligands is observed.[20] The steric hindrance provided by the substituents on the C^N ligands modulates the inter-nuclear distance in the solid state. The shortest inter-iridium distance between adjacent complexes is approximately 7.24 Å in **1a** and increases significantly in **R2** and **2a** (~10.55 and 10.97 Å, respectively). A similar Ir···Ir distance is observed when both R_1 and R_2 are *tert*-butyl groups in **1b** (~10.86 Å). In **R1** the distance 7.897 Å is notably higher with respect to **1a**. The inter-iridium distance for **R3** is with 8.87 Å,[20] which is significantly shorter compare to the distance in **R2** and **2a**.

Cyclic Voltammetry

The electrochemical behaviour of each of the complexes was investigated by cyclic voltammetry (CV) in deaerated MeCN solution at 298 K with *n*-Bu_4NPF_6 as the supporting electrolyte at a scan rate of 100 mV s^{-1} and using ferrocene/ferrocenuim (Fc/Fc^+) as the internal reference. All potentials are referenced with respect to SCE (Fc/Fc^+ = 0.38 V in MeCN).[21] The cyclic voltammograms are shown in Figure **3** and the electrochemistry data are given in Table **1**.

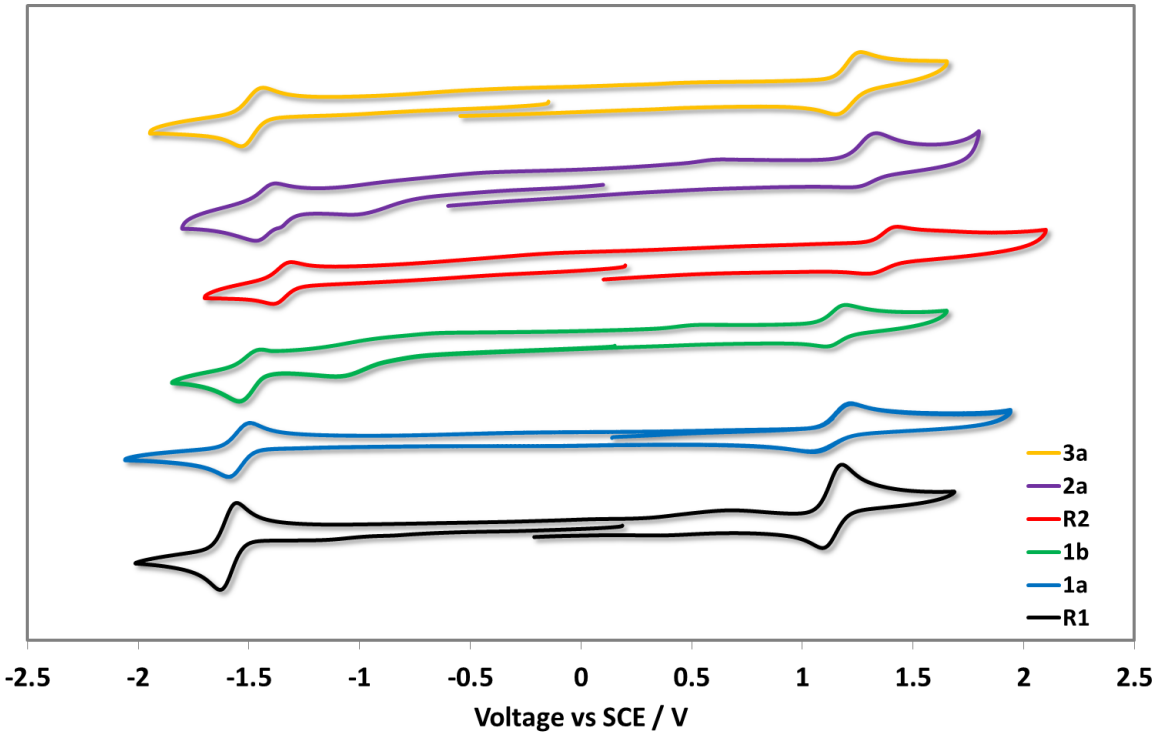

Figure **3.** Cyclic voltammograms of **1a**–**5a** measured in a deaerated MeCN with 0.1 M nBu$_4$NPF$_6$ at a scan rate of 100 mV s^{-1} in the positive scan direction and Fc/Fc$^+$ as the internal standard, and are referenced with respect to SCE (Fc/Fc$^+$ = 0.38 V in MeCN).[21]

Table **1**. Electrochemical data and orbital energies for the investigated complexes[a]

	$E_{1/2}^{ox}$ / V	ΔE_p / mV	$E_{1/2}^{red}$ / V	ΔE_p / mV	E_{HOMO}[b] / eV	E_{LUMO}[b] / eV	ΔE_{redox} / V
R1	1.13	90	-1.61	70	-5.93	-3.20	2.74
1a	1.13	180	-1.54	100	-5.93	-3.26	2.67
1b	1.15	70	-1.52	90	-5.95	-3.29	2.67
R2	1.35	90	-1.37	80	-6.16	-3.43	2.72
2a	1.29	90	-1.43	70	-6.10	-3.38	2.72
3a	1.21	100	-1.49	120	-6.01	-3.37	2.70

[a] Measurements were carried out in degassed MeCN at a scan rate of 100 mV s^{-1} with Fc/Fc^+ used as the internal reference and referenced with respect to SCE (Fc/Fc^+ = 0.38 V in MeCN).[21] [b] $E_{HOMO/LUMO}$ = -[$E^{ox/red}$ vs. Fc/Fc^+ + 4.8] eV.[22]

Each complex displays a quasi-reversible oxidation wave attributed to an admixture of the Ir(III)/Ir(IV) redox couple and contributions from the aryl ring of C^N ligands.[10] The addition of *tert*-butyl groups in **1a** and **1b** renders the oxidation somewhat less reversible compared to the reference **R1** though the oxidation potentials remain essentially unchanged, despite the inductively electron-donating character of this substituent. Upon addition of aryl groups to the 4-pyridyl position, the oxidation waves are anodically shifted, a reflection of the moderately strong electron-withdrawing character of these groups. This anodic shifting is somewhat mitigated by the conjugation present between the 3,5-di-*tert*-butylphenyl substituent and the coordinating pyridine in **3a**, while in **R2** and **2a** the aryl groups are oriented perpendicular as a function of the *o*-methyl substituents on the arene; the magnitude of the inductively electron-withdrawing character of the aryl group is further modulated by the presence of the more strongly electron-donating methoxy substituent in **2a** (E_{ox} = 1.29 V) compared to the methyl substituent in **R2** (E_{ox} = 1.35 V). In CH_2Cl_2, it has been previously shown that **R2** has an oxidation wave at 1.14 V.[8d] Thus, the solvent has a unusually large influence on the oxidation potential of this complex. All complexes display a single quasi-reversible reduction wave within the electrochemical window of MeCN. Despite the consistent assignment that the reduction is localized on the ancillary d*t*Bubpy ligand, the reduction potential varies over a moderately large range from -1.37 V for **R2** to -1.61 V for **R1**. In CH_2Cl_2 **R2** exhibits an irreversible reduction at -1.15 V.[18] The most inductively electron-withdrawing substituents on the C^N ligands induce the greatest shift to less negative potentials in **R2** and **2a**, this via modulation of the electron density on the iridium centre. Analogous to that observed for the

oxidation potentials, this effect is counteracted by the increased conjugation present in **3a**. Surprisingly, despite the electron-donating nature of the *tert*-butyl groups, the reduction potential is not further cathodically shifted, but instead is -1.54 V for **1a** and -1.52 V for **1b**.

UV-Vis absorption spectroscopy

The absorption spectra for all complexes recorded in aerated MeCN at 298 K are shown in Figure **4** and the data summarized in Table **2**.

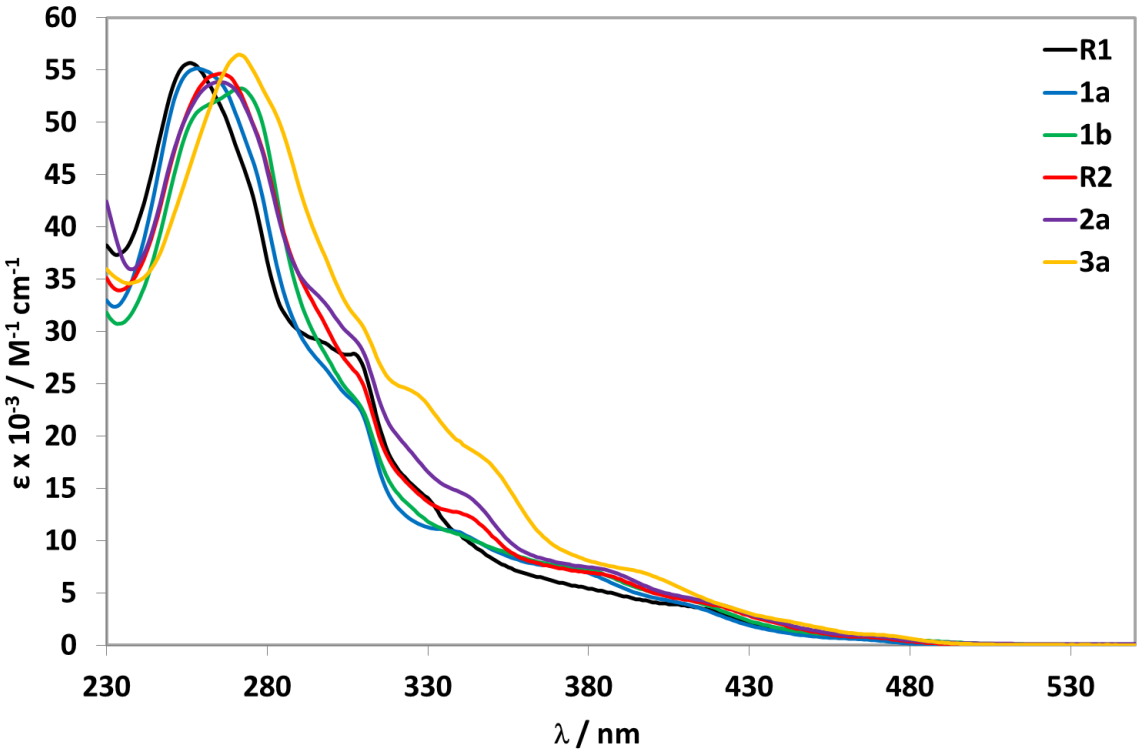

Figure **4**. UV-Vis absorption spectra recorded at 298 K in aerated acetonitrile.

Table **2**. UV-vis absorption data of the investigated Ir(III) complexes

λ_{abs} / nm (ε / M^{-1} cm^{-1})[a]

R1	255 (56 853), 286 (34 421), 309 (28 841), 329 (16 244), 408 (3 757), 466 (663)
1a	258 (55 115), 309 (22 533), 323 (12 442), 340 (10 817), 374 (7 397), 410 (3 976), 448 (941)
1b	272 (53 237), 310 (22 321), 329 (12 109), 377 (7477), 397 (5 357), 410 (4 408), 429 (2 455), 470 (837)
R2	267 (54 540), 310 (24 832), 331 (13 504), 344 (12 153), 385 (6 752), 419 (3 826), 471 (675)
2a	265 (53 788), 296 (33 350), 310 (28 049), 343 (14 195), 385 (7 269), 419 (4 019), 467 (855)
3a	272 (56 407), 311 (29 765), 327 (23 945), 350 (17 179), 402 (6 388), 439 (2 460), 472 (993)

[a] recorded in aerated MeCN at 298 K.

The acquired absorption data for **R1**,[23] **1b**[24] and **R2**[8d] match those previously reported. For all complexes, the electronic absorption spectra show intense (ε on the order of 5.5×10^4 M^{-1} cm^{-1}) high-energy absorption bands between 255 - 272 nm that are assigned to $^1\pi$–π^* ligand-centred (^{1}LC) transitions on both the C^N and N^N ligands. With respect to **R1**, complex **3a** shows a modest red-shift of the ^{1}LC band that is due to the greater conjugation of the 3,5-di-*tert*-butylphenyl ring with the pyridine while a similar red-shifting compared to **R1** of this band is observed for **1b**, also due to LUMO stabilization of the C^N ligands. The profiles of the low-energy bands are found to be insensitive to the nature of the substituents on the C^N ligands. All complexes show moderately intense absorption bands in the range of 300 to 340 nm, which are assigned to spin-allowed mixed metal-to-ligand charge transfer transitions (^{1}MLCT) and ligand-to-ligand charge transfer transitions (^{1}LLCT). Weaker absorption bands are observed beyond 400 nm, tailing to 490 nm. These bands are assigned to spin-forbidden (^{3}MLCT/^{3}LLCT) transitions.[25]

Photophysical Properties

Solution-state Photophysical Behavior

The photoluminescence (PL) spectra in degassed MeCN are shown in Figure **5a** and the data are summarized in Table **3**.

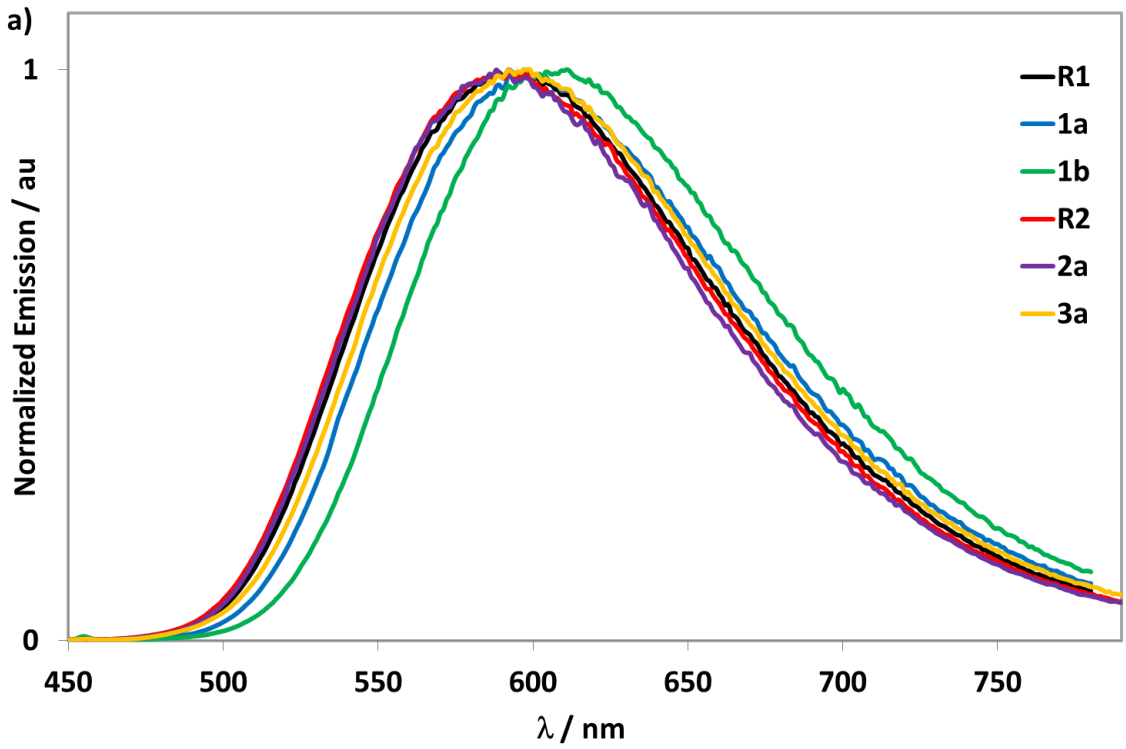

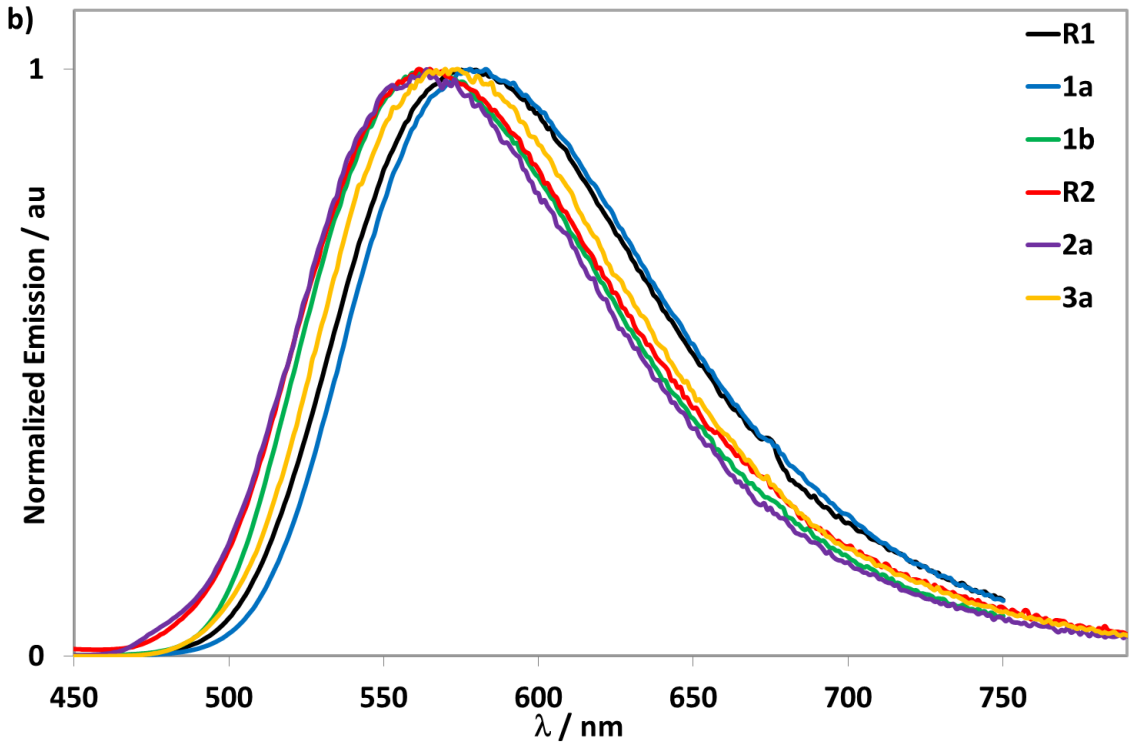

Figure **5.** Emission spectra. a) recorded at 298 K in deaerated MeCN, with λ_{exc} = 400 nm, b) dropcast thin films at 298 K, with λ_{exc} = 400 nm.

Table **3.** Photophysical data of **1a-5a**.

	MeCN					**Neat film**		
	λ_{PL}[a] / nm	τ_{PL}[a] / ns	Φ_{PL}[a,b] / %	k_r[c] × 10^{-5} / s^{-1}	k_{nr}[d] × 10^{-5} / s^{-1}	λ_{PL}[e] / nm	τ_{PL}[e,f] / ns	Φ_{PL}[g] / %
R1	592	581	31	3.61	13.60	578	5 (11.7%) 29 (30.6%) 180 (57.7%)	23
1a	597	497	26	3.42	16.70	579	9 (13.7%) 40 (33.2%) 200 (53.1%)	40

1b	611	250	12	3.20	36.80	565	8 (7.7%) 43 (23.4%) 225 (68.9%)	27
R2	592	643	28	2.95	12.60	565	10 (16.4%) 42 (37.5%) 171 (46.1%)	15
2a	588	623	29	3.05	13.00	564	10 (14.4%) 42 (35.5%) 179 (50.1%)	16
3a	598	501	25	3.39	16.57	570	8 (13.8%) 36 (34.3%) 183 (51.9%)	40

[a] recorded at 298 K in deaerated MeCN, with λ_{exc} = 400 nm; [b] $[Ru(bpy)_3]Cl_2 \cdot 6H_2O$ was used as reference (Φ_{PL} = 0.04 in 10^{-5} M aerated H_2O);[26] [c] $k_r = \tau_{PL} / \Phi_{PL}$. [d] $k_{nr} = 1/(\tau_{PL} - k_r) = [(1 - \Phi_{PL})/ \tau_{PL}]$; [e] values refer to dropcast thin films at 298 K, with λ_{exc} = 400 nm; [f] with contribution of component in parentheses; [g] values refer to dropcast thin films at 298 K using an integration sphere under an N_2 environment.

Upon excitation at 400 nm, all complexes show moderately intense yellow emission over a narrow range between 588 to 611 nm and show a broad and unstructured profile, indicative of an emission with mixed CT character. An increasing red-shifting of the emission spectra is observed upon addition of *tert*-butyl groups (5 nm, 140 cm^{-1} for **R1** to **1a** and 19 nm, 530 cm^{-1} for **1a** to **1b**). This trend is also observed for the LC band in the absorption spectra and correlates as well with a slightly smaller ΔE_{redox} gaps. The effect of the addition of electron-donating groups on the phenyl rings of the C^N ligands has been shown to induce a red-shift of the emission.[23a] A red-shift of 6 nm (169 cm^{-1}) in the emission spectrum is also observed for **3a** compared to **R1**, which is due to stabilization of the triplet state as a result of the increased conjugation within the C^N ligands. Given the orthogonal conformation of the aryl groups in **R2** and **2a** there is expectedly no significant change in the emission energy, consistent with

previous studies.[8b, 8d] This design approach permits a modulation of the bulkiness of the resulting complexes without substantially affecting the emission energy.

The photoluminescence quantum yield (Φ_{PL}) values of all complexes are approximately in the same range (Φ_{PL} ~ 25 – 31%), except for notably red-shifted **1b**, which shows a lower Φ_{PL} of 12%. This finding is a logical consequence of the energy gap law, which states that the non-radiative decay rate increases with decreasing emission energy.[27] These values are comparable to those obtained for related cationic iridium complexes emitting in the same energy region.[3d, 5, 8a, 23a, 24, 28] The emission decays are monoexponential and the lifetimes (τ_{PL}) are all in the submicrosecond regime. The addition of increasing numbers of *tert*-butyl groups on the C^N ligands result in a decrease in the τ_{PL} values, a consequence of an increase in the non-radiative decay rate, k_{nr}. Over the series of substituted complexes, the radiative decay rate, k_r, remains similar, though lower than the reference complex **R1**.

Emission Studies in Neat Films

In order to emulate the emissive layer in the LEEC devices, neat films of all complexes were prepared by drop-casting a dichloromethane solution onto a glass substrate, which was then dried under vacuum. The emission spectra of the neat films were recorded at 298 K open to air (Figure **5b** and Table **3**). All complexes display blue-shifted, broad and unstructured emission spectra (~ 30 nm, 820 cm^{-1}) compared to the MeCN solution measurements. The absence of any red-shifting indicates that there is no excimer formation. Multi-exponential emission decay kinetics are observed for all complexes, with the longest component in each being significantly shorter than the τ_{PL} found in MeCN solution. Photoluminescence quantum yields for **R1**, **R2** and **2a**, remain essentially unchanged compared to solution measurements

while those of **1a**, **1b** and **3a** are enhanced, a function of reduced non-radiative decay in the neat film.

LEEC Devices

LEECs were prepared and the electroluminescence properties of complexes all complexes are shown in Figure **6a-c** while Figure **6d** describes the device architecture. The LEEC data are summarized in Table **4**. The devices were built on ITO-patterned substrates, where poly(3,4-ethylenedioxythiophene):poly(styrenesulfonate) (PEDOT:PSS) layer (80 nm) was deposited by spin-coating. The LEEC active layer (100 nm) was deposited from MeCN by spin-coating, which contained the emitting complex mixed with the ionic liquid (IL) 1-butyl-3-methylimidazolium hexafluorophosphate, [Bmim][PF_6], in a 4:1 molar ratio (complex:IL). Aluminium was evaporated as a top contact electrode. For simplicity, the LEECs are referred as **DR1** to **D3a** containing complex **R1** to **3a**. LEECs were characterized by applying a bias and monitoring the emitted light over time. Unlike LEECs measured at constant voltage (DC), pulsed-current LEECs show faster response and improved device lifetime.[29] The devices were characterized under an inert atmosphere by applying an average pulsed current (1 kHz, 50% duty cycle) of 100 A m^{-2}.

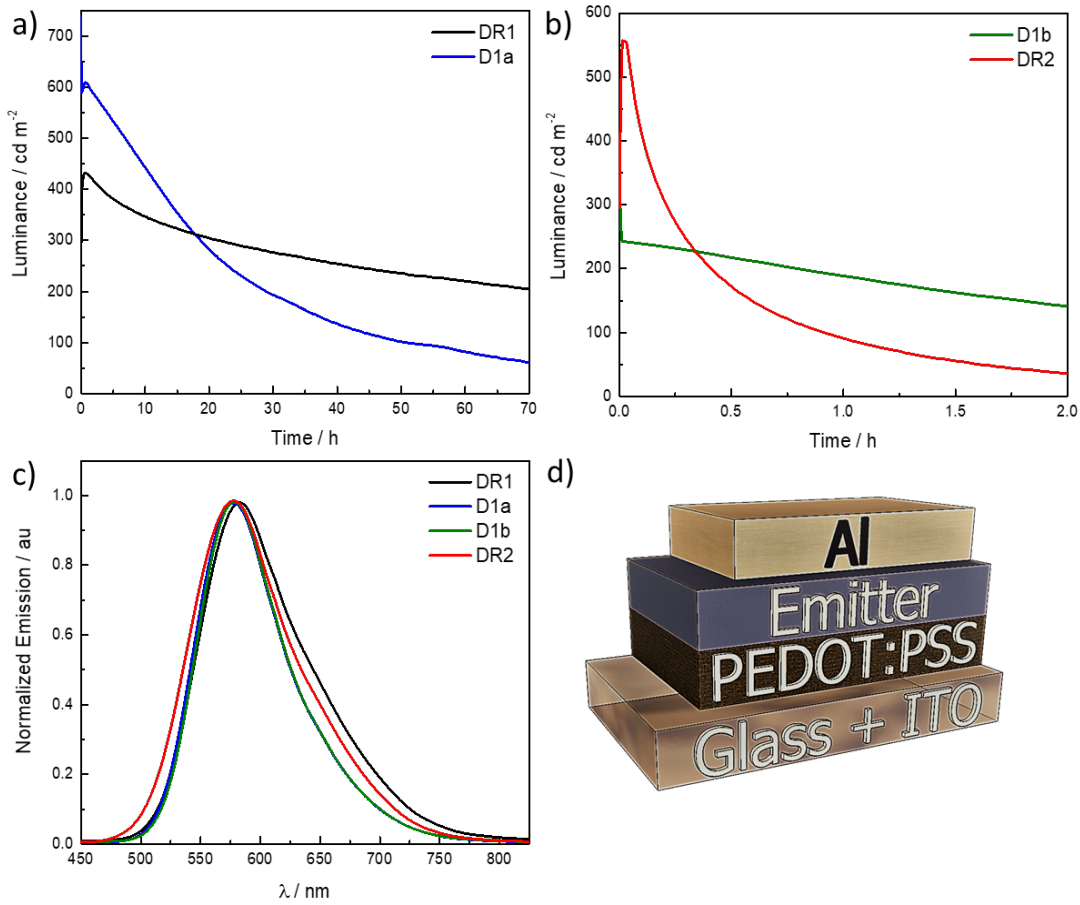

Figure **6.** Luminance versus time (**DR1** and **D1a** in (a) and **D1b** and **DR2** in (b)) operated with a pulsed current of 100 A m^{-2} (1KHz, 50% duty cycle and block wave). (c) Electroluminescence spectrum. (d) LEEC architecture.

The yellow electroluminescence of the devices consists on one peak centred at 582 nm for **DR1** and 577-578nm for **D1a**, **D1b** and **DR2** (see Figure **6c**). The electroluminescence spectra are narrower than the thin film photoluminescence spectra. The solubility of the **D2a** and **D3a** was poor (<15 mg mL^{-1}) in both MeCN and CH_2Cl_2, which led to poor morphology quality of the spin-coated films and devices with high leakage currents. Even when the solution is filtered (200 nm porous size), the saturated solutions form grains during the solvent

evaporation by spin-coating, which was confirmed by optical microscopy (see Figure **S25** in the Supporting Information).

The LEECs **DR1, D1a, D1b** and **DR2** exhibit instantaneous luminance that increases rapidly leading to short turn-on time (t_{on}) of less than one minute, which is defined as the time to reach the maximum luminance, except **DR1** where ton is 2400 s. The long t_{on} is related with a slow evolution of the charge current equilibrium. A slow growth of the doped regions delays degradation and slows down the exciton-quenching rates.[30] That would lead to more stable devices. In fact, **DR1** has the highest $t_{1/2}$. The devices are bright, with maximum luminance values in the same order of magnitude, between 350 and 750 cd m^{-2} across all devices. The devices are moderately efficient, with a maximum efficacy of 7.4 cd A^{-1} in the case of **D1a**. Lower efficiencies are achieved for **D1b**, **DR1** and **DR2**, following the trend in the photoluminescence quantum yield of the thin film. However, the LEECs differs in terms of their stability, defined as time to reach half of the maximum luminance. **DR1** has a lifetime above 62 hours, which makes it the most stable device within this study, maintaining almost constant the luminance over the time about 300 cd m^{-2}. **D1a** has a higher luminance (737 cd m^{-2}) although it is achieved only during few seconds and then proceeds to drop to ~600 cd m^{-2}, lasting for only 14 h. **D1b** and **DR2** present low stabilities. Initially **D1b** displays luminance values around 350 cd m^{-2} but is stable for 1.3 h. **DR2** shows higher turn-on luminance (~550 cd m^{-2}) however, the emission drops fast and the $t_{1/2}$ only 0.3 h. The result comparison with previous works is complicated as the operational parameters are different.[12] Pulse current is used to improve the device stability compared to what is obtained using a constant voltage driving. The limited stability of these devices relates in part to poor film-forming characteristics, leading to a morphology with imperfections, such as tiny dots. This was in particular the case for the films prepared with complexes **2a** and **3a** (SI). Even though such

imperfections were not identified for the films of the other complexes it is likely due to the similarity in the chemical structure that also here some film-forming issues are occurring, albeit at a smaller scale and dimension. This would also lead to pathways where the degradation is accelerated. Higher photoluminescence quantum yield values were published for similar complexes.[8a] The described imperfections in the film formation can explain the lower observed photoluminescence quantum yield. However, the obtained EQEs (1.2% – 2.6%) are in line with the typical values for efficient yellow LEECs. Indeed, only a few examples with high EQE (>6%) have been published for yellow/orange LEECs.[3a, 3d, 31] Furthermore, the EQE's appear in line with the PLQY of the films, again highlighting the main issue is the film formation.

Table **4.** Device performance of the LEEC: ITO/PEDOT:PSS/Complex:[Bmim][PF_6]/Al operated with a pulsed current of 100 A m^{-2} (1KHz, 50% duty cycle and block wave).

Device	**Lum_{max} / cd m^{-2}**	**t_{on} / s**	**$t_{1/2}$ / h**	**Efficacy / cd A^{-1}**	**PE / lm W^{-1}**	**EQE / %**	**λ_{EL} / nm**	**CIE (x, y)**
DR1	432	2400	62	4.3	2.3	1.8	582	0.50, 0.52
D1a	737	25	14	7.4	3.7	2.6	577	0.49, 0.50
D1b	353	<5	1.3	3.4	1.4	1.2	578	0.51, 0.51
DR2	557	54	0.3	5.6	2.1	2	578	0.47, 0.51

[a]Maximum luminance. [b]Time to reach maximum luminance. [c]Time to reach one-half of the maximum luminance. [d]Maximum efficacy. [e]Maximum power efficiency. [f]Maximum external quantum efficiency. [g]Wavelength emission in electroluminescence. [h]CIE coordinates obtained from the electroluminescence spectrum at maximum luminance.

Conclusions

In conclusion, we successfully synthesized and characterized a series of cationic Ir(III) complexes of the form $[Ir(C^N)_2(dtBubpy)]PF_6$ incorporating bulky substituents on the C^N ligand in order to develop new emissive materials for light-emitting electrochemical cells. The syntheses are straightforward allowing the introduction of *tert*-butyl, mesityl, manisyl, and 3,5-di-*tert*-butylphenyl groups into the C^N ligand. This systematic study revealed that the solubility of the complexes in standard organic solvents increased. At high concentrations (>15 mg mL^{-1}) complexes **2a** and **3a** did not, however, show good solubility in MeCN and DCM. All complexes have been structurally characterised and the single crystal structure determinations of complexes **1a**, **1b**, **R2** and **3a** confirm that by increasing the sterical congestion of the substituent the inter-nuclear distance between adjacent complexes increased in the solid state. All complexes show bright yellow luminescence in MeCN, with moderate photoluminescence quantum yields. The yellow phosphorescence of the parent complex **R1** is retained, due to a twisted conformation of the bulky aromatic substituents (in **R2**, **2a** and **3a**) as they do not extend the π-conjugated system of the C^N ligand. Neat film photoluminescence quantum yields of up to 40% could be obtained. Complexes **R1**, **1a**, **1b** and **R2** were successfully employed in LEECs, showing yellow luminescence with moderate external quantum efficiencies.

Experimental Section

Synthesis

The compounds **ClR2** and **LR2** where synthesised according previously reported procedures.[8b]

General procedure I (for L1a and L1b)

A solution of *tert*-butylpyridine (1.0 equiv.) in CH_2Cl_2 was stirred at room temperature. Trifluoroacetic acid (1.0 equiv.) was added followed by phenylboronic acid (1.5 equiv.), water (12 mL), a solution of silver(I) nitrate (0.2 equiv.) in 8 mL of water and potassium persulfate

(3.0 equiv.). The solution was stirred vigorously for 6 h. The reaction was quenched with water (10 mL), extracted with CH_2Cl_2 (50 mL) and washed with conc. aqueous $NaHCO_3$ (10 mL). After layer separation, the brown yellow organic phase was dried over $MgSO_4$ and the solvent was evaporated under vacuum leaving brown oil which was purified on silica (10% of EtOAc in petroleum ether). The desired fractions were combined and reduced until dryness yielding the desired compound as oil.

4-(*tert*-butyl)-2-phenylpyridine (L1a)

Compound **L1a** was prepared following the general procedure I and was obtained as yellow-brown oil (0.351 g, 1.661 mmol). **Yield:** 45%, **R_f:** 0.32 (10% of EtOAc in petroleum ether on silica). **^{1}H NMR** (400 MHz, $CDCl_3$) δ 8.62 (d, 1H), 8.02 – 7.93 (m, 2H), 7.74 – 7.69 (m, 1H), 7.48 (q, *J* = 7.4 Hz, 2H), 7.41 (q, *J* = 7.4 Hz, 1H), 7.25 – 7.22 (m, 1H), 1.36 (s, 9H). **^{13}C NMR** (101 MHz, CDCl3) δ 161.4, 156.3, 148.9, 140.2, 129.7, 129.4, 125.9, 118.5, 116.8, 33.7, 31.2. **HR-MS** ($FTMS^+$)**: $[M-H]^+$ Calculated:** ($C_{15}H_{17}NH$): 212.1434 **Found:** 212.1428. The characterisation matches that previously reported.[16]

4-(*tert*-butyl)-2-(4-(*tert*-butyl)phenyl)pyridine (L1b)

Compound **L1b** was prepared following the general procedure I and was obtained as yellow-brown oil (1.000 g, 3.739 mmol). **Yield:** 46%, **R_f:** 0.36 (10% EtOAc in petroleum ether on silica). **^{1}H NMR** (400 MHz, $CDCl_3$) δ 8.55 (d, 1H), 7.89 (d, *J* = 8.3 Hz, 2H), 7.68 (s, 1H), 7.49 (d, *J* = 8.3 Hz, 2H), 7.22 – 7.20 (m, 1H), 1.52 (s, 18H). The matches that previously reported.[32]

General procedure II (for Cl2a and Cl3a)

A mixture of 2-chloro-4-iodopyridine (1.00 equiv.), the corresponding arylboronic acid (1.30 equiv.), 2 M aqueous K_2CO_3 (5.00 equiv.) and 1,4-dioxane (35 mL) was degassed for 15 min. $Pd(Ph_3)_4$ (0.04 equiv.) was added, and the reaction mixture was stirred at 95 °C for 3 days, then

cooled to room temperature. Toluene (80 mL) was added. After layer separation the organic phase was washed with water (10 mL) and dried over $MgSO_4$. The solvent was evaporated leaving a residue which was purified by column chromatography (15% EtOAc in petroleum ether on silica). The desired fractions were combined, and the solvent evaporated leaving the title compound as solid.

2-chloro-4-(4-methoxy-2,6-dimethylphenyl)pyridine (Cl3a)

Compound **Cl3a** was prepared following the general procedure II and was obtained as a colourless sticky oil (0.995 g, 4.016 mmol). **Yield:** 94%. **R_f:** 0.32 (10% EtOAc in petroleum ether on silica). **^{1}H NMR** (400 MHz, Chloroform-*d*) δ = 8.44 (d, *J*=5.0, 1H), 7.15 (m, 1H), 7.04 (d, *J*=5.0, 1H), 6.95 (s, 2H), 2.33 (s, 3H), 2.00 (s, 6H). **^{13}C NMR** (101 MHz, $CDCl_3$) δ = 159.2, 152.7, 151.8, 149.7, 136.6, 130.4, 125.5, 124.0, 113.1, 77.4, 77.2, 77.0, 76.7, 55.2, 20.9. **HR-MS** ($FTMS^+$)**: [M-H]$^+$ Calculated:** ($C_{14}H_{15}ClNOH$): 248.0837 **Found:** 248.0837. **CHN**: **Calcd.** for $C_{14}H_{14}ClNO$: C, 67.88; H, 5.70; N, 5.65. **Found:** C, 67.76; H, 5.59; N, 5.57.

2-chloro-4-(3,5-di-*tert*-butylphenyl)pyridine (Cl3a)

Before following the general procedure II for **Cl3a**, (3,5-di-*tert*-butylphenyl)boronic acid was prepared, adapted from a previously reported procedure.[33]

Cl3a was obtained as a red solid (1.613 g, 5.346 mmol). **Yield:** 96%. **R_f:** 0.40 (10 vol.% EtOAc in petroleum ether on silica). **Mp:** 68 °C. **^{1}H NMR** (400 MHz, Chloroform-*d*) δ = 8.42 (d, 1H), 7.54 (d, 2H), 7.41 (m, 3H), 1.38 (s, 18H). **^{13}C NMR** (101 MHz, $CDCl_3$) δ = 152.8, 152.0, 151.9, 149.8, 136.4, 123.8, 122.3, 121.4, 120.8, 35.0, 31.4. **HR-MS** ($FTMS^+$)**: [M-H]$^+$ Calculated:** ($C_{19}H_{25}ClNH$): 302.1670 **Found:** 302.1668. **CHN**: **Calcd.** for $C_{19}H_{24}ClN$: C, 75.60; H, 8.01; N, 4.64. **Found:** C, 75.41; H, 7.93; N, 4.61.

General procedure III (for L2a and L3a)

A mixture of the corresponding 2-chloro-4-arylpyridine (1.00 equiv.), phenylboronic acid (1.50 equiv.), palladium (II) acetate (0.06 equiv.), PPh_3 (0.26 equiv.), 2 M aqueous Na_2CO_3 (4.00 equiv.) and 1,2-dimethoxyethane (25 mL) was degassed for 15 min. The reaction mixture was heated to reflux for 24 h under Ar atmosphere, and then cooled to room temperature. CH_2Cl_2 (50 mL) was added. After layer separation the organic layer was washed with brine and dried over $MgSO_4$. The solvent was evaporated leaving a residue, which was purified by column chromatography (10% petroleum ether in CH_2Cl_2). The desired fractions were combined, and the solvent evaporated leaving the desired compound as a solid.

4-(4-methoxy-2,6-dimethylphenyl)-2-phenylpyridine (L2a)

Compound **L2a** was prepared according to the general procedure III and was obtained as a colourless solid (0.420 g, 1.451 mmol). **Yield:** 89%. **R_f:** 0.25 (10 vol.% EtOAc in petroleum ether on silica). **Mp.:** 57-58 °C. **^{1}H NMR** (400 MHz, Chloroform-*d*) δ = 8.70 (dd, *J*=4.9, 1H), 8.00 (m, 2H), 7.55 (s, 1H), 7.46 (m, 3H), 7.06 (dd, *J*=4.9, 1H), 6.72 (s, 2H), 3.93 (s, 3H), 2.21 (s, 6H). **^{13}C NMR** (101 MHz, $CDCl_3$) δ = 158.9, 157.6, 150.2, 149.8, 139.3, 136.8, 131.9, 129.0, 128.7, 126.9, 123.6, 121.9, 113.0, 77.4, 77.0, 76.7, 55.2, 21.0. **HR-MS** ($FTMS^+$)**: $[M-H]^+$ Calculated:** ($C_{20}H_{19}NOH$): 290.1539 **Found:** 290.1538. **CHN**: **Calcd.** for $C_{20}H_{19}NO$: C, 83.01; H, 6.62; N, 4.84. **Found:** C, 82.89; H, 6.56; N, 4.73.

4-(3,5-di-*tert*-butylphenyl)-2-phenylpyridine (L3a)

Compound **L3a** was prepared following the general procedure III and was obtained as a colourless solid (0.751 g, 2.186 mmol). **Yield:** 85%. **R_f:** 0.22 (5 vol.% EtOAc in petroleum ether on silica). **Mp.:** 72-75 °C **^{1}H NMR** (400 MHz, $CDCl_3$) δ = 8.73 (d, 1H), 8.05 (d, 2H), 7.90 (s, 1H), 7.52 (m, 5H), 7.45 (d, 2H), 1.40 (s, 18H). **^{13}C NMR** (101 MHz, Chloroform-d) δ

= 150.0, 129.0, 128.9, 127.2, 123.3, 121.6, 120.9, 119.3, 31.6. **HR-MS** ($FTMS^+$)**:** $[M-H]^+$ **Calculated:** ($C_{25}H_{29}NH$): 344.2371 **Found:** 344.2373. **CHN**: **Calcd.** for $C_{25}H_{29}N$: C, 87.41; H, 8.51; N, 4.08. **Found:** C, 87.31; H, 8.43; N, 4.14.

General procedure IV (for the Synthesis of target Complexes)

The iridium chloride (2.0 equiv.) and the corresponding C^N ligand (5.0 equiv.) were suspended in a mixture of 2-ethoxyethanol/water (75/25). The mixture was refluxed under stirring. After 24 h the mixture was allowed to cool to r.t. and distilled water was added. A precipitate was observed. The solid was washed with Et_2O, H_2O and dried under vacuum to give the intermediate $[Ir(C^N)_2Cl]_2$. A suspension of this dimer (1.0 equiv.), the ancillary ligand 4,4'-di-*tert*-butyl-2,2'-bipyridine (2.2 equiv.) and $AgPF_6$ (2.5 equiv.) in 1,2-dichloroethane was kept at reflux for 2 h and stirred at r.t. for another 16 h. The solvent was then evaporated leaving a brown yellow residue, which was then placed in dichloromethane. A beige precipitate was observed. After filtration, the filtrate was reduced till dryness under reduced pressure, leaving a yellow-brown solid, which was purified on silica with dichloromethane and increasing percentages of methanol (0% - 8%). The desired fractions were collected and reduced to dryness, giving a yellow solid, which was suspended under stirring in a hexane/Et_2O mixture (1/1) for 4 h. The yellow precipitate was filtered off and dissolved in methanol. An aqueous NH_4PF_6 solution was added dropwise resulting in a precipitate. The suspension was stirred vigorously for 2 h and subsequently filtered. The solid was dissolved in CH_2Cl_2 and washed with water. The layers were separated, and the organic layer was reduced to dryness, leaving a yellow solid, which was recrystallised through vapor diffusion using CH_2Cl_2 as the solvent and Et_2O as the anti-solvent. After filtration, the target complexes were obtained as solids.

[Ir(2-phenylpyridinato)$_2$(4,4'-di-*tert*-butyl-2,2'-bipyridine)]PF_6 (R1)

Yellow solid. **Yield:** 89%. **Mp.:** 285 - 290 °C. **Lit.:** 284 - 288 °C.[8a] **^{1}H NMR** (400 MHz, Chloroform-*d*) δ = 8.38 (m, 2H), 7.88 (d, *J*=8.1, 2H), 7.82 (d, *J*=5.8, 2H), 7.74 (t, *J*=7.9, 2H), 7.66 (d, *J*=7.6, 2H), 7.61 (d, *J*=5.8, 2H), 7.37 (dd, *J*=5.9, 1.8, 2H), 7.08 (s, 1H), 7.01 (t, *J*=7.4, 2H), 6.89 (t, *J*=7.4, 2H), 6.29 (d, *J*=7.4, 2H), 1.43 (s, 18H). **^{13}C NMR** (126 MHz, $CDCl_3$) δ = 167.5, 163.8, 155.7, 150.8, 149.6, 149.1, 143.6, 137.9, 131.7, 130.6, 125.2, 124.5, 123.5, 122.3, 121.7, 119.3, 35.7, 30.2. **HR NSI+ MS: $[M\text{-}PF_6]^+$ Calculated:** ($C_{40}H_{40}IrN_4$): 767.2853 **Found:** 767.2836. **CHN**: Calcd. for $C_{40}H_{40}F_6IrN_4P$ x 1/4 CH_2Cl_2: C, 51.69; H, 4.37, N, 5.99. Found: C, 52.04; H, 4.26; N, 5.83. The characterisation matches that previously reported.[12a]

[Ir(4-*tert*-butyl-2-phenylpyridinato)$_2$(4,4'-di-*tert*-butyl-2,2'-bipyridine)][PF_6] (1a)

Yellow solid. **Yield:** 82%. **Mp:** 340 °C (decomp.). **^{1}H NMR** (400 MHz, Chloroform-*d*) δ = 8.39 (d, *J*=1.9, 2H), 7.84 (m, 4H), 7.67 (m, 2H), 7.39 (m, 4H), 7.09 (m, 2H), 7.00 (m, 2H), 6.90 (m, 2H), 6.27 (m, 2H), 1.43 (s, 18H), 1.36 (s, 18H). **^{13}C NMR (101 MHz, Chloroform-*d*)** δ = 167.0, 163.8, 162.3, 155.8, 151.0, 149.81, 148.3, 144.0, 131.8, 130.4, 125.1, 124.2, 122.1, 121.7, 121.2, 116.1, 77.2, 35.7, 35.2, 30.5, 30.4, 30.3. **NSI+ HRMS MS: $[M\text{-}PF_6]^+$ Calculated:** ($C_{48}H_{56}IrN_4$): 879.4105 **Found:** 879.4093. **CHN**: Calcd. for $C_{48}H_{56}F_6IrN_4P$: C, 56.18; H, 5.50, N, 5.46. Found: C, 56.09; H, 5.36; N, 5.44

[Ir(4-*tert*-butyl-2-(4-(*tert*-butyl)phenyl)pyridinato)$_2$(4,4'-di-*tert*-butyl-2,2'-bipyridine)][PF_6] (1b)

Yellow solid. **Yield:** 85%. **Mp:** 345 °C (decomp.).**^{1}H NMR** (400 MHz, Chloroform-*d*) δ = 8.35 (s, 2H), 7.79 (s, 4H), 7.54 (s, 2H), 7.49 (d, 2H), 7.38 (s, 2H), 7.10 (d, 2H), 7.01 (d, 2H), 6.22 (s, 2H), 1.60 (s, 18H), 1.51 (s, 18H), 1.23 (s, 18H). **^{13}C NMR** (101 MHz, Chloroform-d) δ = 167.5, 163.4, 162.1, 155.9, 153.1, 150.9, 65.8, 35.6, 35.1. **NSI+ HRMS MS: [M-PF6]$^+$ Calculated:** ($C_{56}H_{72}IrN_4$): 991.5357 **Found:** 991.5339. **CHN**: **Calcd.** for $C_{48}H_{56}F_6IrN_4P$ x 3/4

CH_2Cl_2: C, 53.72; H, 5.32, N, 5.14. **Found:** C, 53.44; H, 5.26; N, 5.14. The characterisation matches that reported.[24]

[Ir(4-mesityl-2-phenylpyridinato)$_2$(4,4'-di-*tert*-butyl-2,2'-bipyridine)][PF_6] (R2)

Yellow solid. **Yield:** 79%. **Mp.:** 263 - 267 °C. **Lit.:** 264 - 268 °C.[8a] **^{1}H NMR (400 MHz, Chloroform-*d*)** δ = 8.56 (s, 2H), 7.96 (d, 2H), 7.70 (m, 4H), 7.63 (d, 2H), 7.45 (m, 2H), 6.96 (m, 11H), 6.41 (d, 2H), 2.36 (s, 6H), 2.14 (s, 6H), 1.96 (s, 6H), 1.47 (s, 18H). **^{13}C NMR** (126 MHz, $CDCl_3$) δ = 167.65, 164.15, 155.98, 151.81, 151.04, 149.74, 149.05, 143.80, 138.24, 135.08, 134.91, 131.69, 130.70, 128.58, 128.53, 125.17, 124.84, 124.57, 122.39, 122.23, 120.49, 35.80, 30.26, 29.72, 21.08, 20.53, 20.44. **NSI+ HRMS MS: $[M\text{-}PF_6]^+$ Calculated:** ($C_{58}H_{60}IrN_4$): 1003.4418 **Found:** 1003.4411. **CHN**: **Calcd.** for $C_{58}H_{60}F_6IrN_4P$: C, 60.56; H, 5.26, N, 4.87. **Found:** C, 60.49; H, 5.13; N, 5.04. The characterisation matches that previously reported.[8a, 8d]

[Ir(4-(4-methoxy-2,6-dimethylphenyl)-2-phenylpyridinato)$_2$(4,4'-di-*tert*-butyl-2,2'-bipyridine)][PF_6] (2a)

Yellow solid. **Yield:** 75%. **Mp.:** 330 °C (decomp.). **^{1}H NMR** (400 MHz, Chloroform-d) δ = 8.60 (d, J=5.3, 2H), 8.53 (m, 2H), 8.40 (m, 2H), 7.94 (m, 2H), 7.68 (s, 2H), 7.64 (s, 2H), 7.61 (d, 2H), 7.42 (d,2H), 7.31 (d, 2H), 7.01 (s, 2H), 6.93 (s, 2H), 6.91 (s, 2H), 6.69 (d, 4H), 6.38 (d, 2H), 3.82 (s, 6H), 2.14 (s, 6H), 1.96 (s, 6H), 1.45 (s, 18H). **^{13}C NMR** (101 MHz, Chloroform-d) δ = 167.5, 159.3, 155.9, 151.6, 149.7, 149.0, 131.7, 130.6, 130.5, 125.2, 124.5, 122.3, 122.0, 120.8, 113.1, 77.2, 55.2, 35.7, 30.2, 20.8. **NSI+ HRMS MS: $[M\text{-}PF_6]^+$ Calculated:** ($C_{58}H_{60}IrN_4O_2$): 1035.4317 **Found:** 1035.4294. **CHN**: Calcd. for $C_{58}H_{60}F_6IrN_4P$: C, 58.92; H, 5.12, N, 4.74. **Found**: C, 59.00; H, 5.22; N, 4.67.

[Ir(4-(3,5-di-*tert*-butylphenyl)-2-phenylpyridinato)$_2$(4,4'-di-*tert*-butyl-2,2'-pipyridine)][PF_6] (3a)

Yellow solid. **Yield:** 89%. **Mp:** 365 °C (decomp.). **^{1}H NMR** (300 MHz, Chloroform-d) δ = 8.48 (d, J=1.6, 2H), 8.09 (d, J=1.7, 2H), 7.92 (d, J=5.9, 2H), 7.80 (d, J=6.9, 2H), 7.64 (d, J=6.1, 2H), 7.55 (m, 6H), 7.43 (dd, J=5.9, 1.8, 2H), 7.35 (d, J=2.0, 2H), 7.08 (m, 2H), 6.97 (t, J=6.8, 2H), 6.47 (d, J=6.7, 2H), 1.47 (s, 18H), 1.41 (s, 36H). **^{13}C NMR** (126 MHz, Chloroform-*d*) δ = 167.4, 155.8, 151.9, 151.1, 149.7, 148.9, 136.2, 131.9, 130.5, 125.2, 124.4, 124.2, 122.2, 121.8, 121.4, 117.0, 35.7, 35.1, 31.4, 30.2, 29.7. **NSI+ HRMS MS: [M-PF_6]$^+$ Calculated:** ($C_{68}H_{80}IrN_4$): 1143.5954 **Found:** 1143.5983. **CHN**: **Calcd.** for $C_{68}H_{80}F_6IrN_4P$: C, 63.28; H, 6.25, N, 4.34. **Found:** C, 63.23; H, 6.15, N, 4.40

Acknowledgments

We thank Umicore AG for the gift of materials. We thank the EPSRC UK National Mass Spectrometry Facility at Swansea University for analytical services. C.H. acknowledges the *Région Bretagne*, France for funding. E.Z.-C. acknowledges the University of St Andrews and EPSRC (EP/M02105X/1) for financial support.

Supporting information. NMR spectra for ligands and complexes; Supplementary crystallographic data (CCDC: 1034962, 1038996, 1039805 and 1045877); Supplementary LEEC fabrication data.

References

(1). (a) R. C. Evans, P. Douglas and C. J. Winscom, *Coord. Chem. Rev.*, 2006, **250**, 2093-2126; (b) A. F. Henwood and E. Zysman-Colman, *Chem. Commun.*, 2017, **53**, 807-826; (c) S. Ladouceur and E. Zysman-Colman, *Eur. J. Inorg. Chem.*, 2013, **2013**, 2985-3007; (d) K. P. S. Zanoni, R. L. Coppo, R. C. Amaral and N. Y. Murakami Iha, *Dalton Trans.*, 2015, **44**, 14559-14573; (e) M. S. Lowry and S. Bernhard, *Chem. Eur. J.*, 2006, **12**, 7970-7977.

(2). (a) H. Xu, R. Chen, Q. Sun, W. Lai, Q. Su, W. Huang and X. Liu, *Chem. Soc. Rev.*, 2014, **43**, 3259-3302; (b) E. Longhi and L. De Cola, in *Iridium(III) in Optoelectronic and Photonics Applications*, ed. E. Zysman-Colman, John Wiley & Sons, Ltd, 2017, pp. 205-274; (c) J.-H. Jou, S. Kumar, A. Agrawal, T.-H. Li and S. Sahoo, *J. Mater. Chem. C*, 2015, **3**, 2974-3002; (d) D. Ma, T. Tsuboi, Y. Qiu and L. Duan, *Adv Mater*, 2017, **29**, 1603253.

(3). (a) A. F. Henwood and E. Zysman-Colman, in *Iridium(III) in Optoelectronic and Photonics Applications*, John Wiley & Sons, Ltd, 2017, pp. 275-357; (b) S. B. Meier, D. Tordera, A. Pertegás, C. Roldán-Carmona, E. Ortí and H. J. Bolink, *Mater. Today*, 2014, **17**, 217-223; (c) C. E. Housecroft and E. C. Constable, *Coord. Chem. Rev.*, 2017, **350**, 155-177; (d) A. F. Henwood and E. Zysman-Colman, *Top. Curr. Chem.*, 2016, **374**, 36.

(4). For recent reviews on LEECs see: R. D. Costa, E. Ortí, H. J. Bolink, F. Monti, G. Accorsi and N. Armaroli, *Angew. Chem. Int. Ed.*, 2012, **51**, 8178-8211.

(5). H. C. Su, F. C. Fang, T. Y. Hwu, H. H. Hsieh, H. F. Chen, G. H. Lee, S. M. Peng, K. T. Wong and C. C. Wu, *Adv. Funct. Mater.*, 2007, **17**, 1019-1027.

(6). G. G. Malliaras, J. D. Slinker, J. A. DeFranco, M. J. Jaquith, W. R. Silveira, Y.-W. Zhong, J. M. Moran-Mirabal, H. G. Craighead, H. D. Abruna and J. A. Marohn, *Nat Mater*, 2008, **7**, 168-168.

(7). V. N. Kozhevnikov, Y. Zheng, M. Clough, H. A. Al-Attar, G. C. Griffiths, K. Abdullah, S. Raisys, V. Jankus, M. R. Bryce and A. P. Monkman, *Chem. Mater.*, 2013, **25**, 2352-2358.

(8). (a) D. R. Martir, C. Momblona, A. Pertegás, D. B. Cordes, A. M. Z. Slawin, H. J. Bolink and E. Zysman-Colman, *ACS Applied Materials & Interfaces*, 2016, **8**, 33907-33915; (b) D. Rota Martir, A. K. Bansal, V. Di Mascio, D. B. Cordes, A. F. Henwood, A. M. Z. Slawin, P. C. J. Kamer, L. Martinez-Sarti, A. Pertegas, H. J. Bolink, I. D. W. Samuel and E. Zysman-Colman, *Inorganic Chemistry Frontiers*, 2016, **3**, 218-235; (c) A. F. Henwood, A. K. Bansal, D. B. Cordes, A. M. Z. Slawin, I. D. W. Samuel and E. Zysman-Colman, *J. Mater. Chem. C*, 2016, **4**, 3726-3737; (d) D. Rota Martir, G. J. Hedley, D. B. Cordes, A. M. Z. Slawin, D. Escudero, D. Jacquemin, T. Kosikova, D. Philp, D. M. Dawson, S. E. Ashbrook, I. D. W. Samuel and E. Zysman-Colman, *Dalton Trans.*, 2016, **45**, 17195-17205.

(9). K. J. Suhr, L. D. Bastatas, Y. Shen, L. A. Mitchell, B. J. Holliday and J. D. Slinker, *ACS Appl Mater Interfaces*, 2016, **8**, 8888-8892.

(10). A. M. Bünzli, E. C. Constable, C. E. Housecroft, A. Prescimone, J. A. Zampese, G. Longo, L. Gil-Escrig, A. Pertegás, E. Ortí and H. J. Bolink, *Chem. Sci.*, 2015, **6**, 2843-2852.

(11). (a) H. J. Bolink, E. Coronado, R. n. D. Costa, N. Lardiés and E. Ortì, *Inorg. Chem.*, 2008, **47**, 9149-9151; (b) A. B. Tamayo, S. Garon, T. Sajoto, P. I. Djurovich, I. M. Tsyba, R. Bau and M. E. Thompson, *Inorg. Chem.*, 2005, **44**, 8723-8732.

(12). (a) J. D. Slinker, A. A. Gorodetsky, M. S. Lowry, J. Wang, S. T. Parker, R. Rohl, S. Bernhard and G. G. Malliaras, *J. Am. Chem. Soc.*, 2004, **126**, 2763; (b) L. Sun, A. Galan, S. Ladouceur, J. D. Slinker and E. Zysman-Colman, *J. Mater. Chem.*, 2011, **21**, 18083-18088.

(13). R. D. Costa, E. Ortı´, H. J. Bolink, S. Graber, C. E. Housecroft and E. C. Constable, *J. Am. Chem. Soc.*, 2010, **132**, 5987-5989.

(14). H. J. Bolink, E. Coronado, R. D. Costa, E. Ortì, M. Sessolo, S. Graber, K. Doyle, M. Neuburger, C. E. Housecroft and E. C. Constable, *Adv. Mater.*, 2008, **20**, 3910-3913.

(15). R. D. Costa, E. Ortí, H. J. Bolink, S. Graber, C. E. Housecroft and E. C. Constable, *Adv. Funct. Mater.*, 2010, **20**, 1511-1520.

(16). I. B. Seiple, S. Su, R. A. Rodriguez, R. Gianatassio, Y. Fujiwara, A. L. Sobel and P. S. Baran, *J. Am. Chem. Soc.*, 2010, **132**, 13194-13196.

(17). M. Nonoyama, *Bull. Chem. Soc. Jpn.*, 1974, **47**, 767-768.

(18). M. Lepeltier, T. K.-M. Lee, K. K.-W. Lo, L. Toupet, H. Le Bozec and V. Guerchais, *Eur. J. Inorg. Chem.*, 2005, **2005**, 110-117.

(19). For recent reviews see: L. Flamigni, A. Barbieri, C. Sabatini, B. Ventura and F. Barigelletti, *Top. Curr. Chem.*, 2007, **281**, 143-203.

(20). K. J. Suhr, L. D. Bastatas, Y. Shen, L. A. Mitchell, G. A. Frazier, D. W. Taylor, J. D. Slinker and B. J. Holliday, *Dalton Trans*, 2016, **45**, 17807-17823.

(21). V. V. Pavlishchuk and A. W. Addison, *Inorg. Chim. Acta*, 2000, **298**, 97-102.

(22). C. M. Cardona, W. Li, A. E. Kaifer, D. Stockdale and G. C. Bazan, *Adv. Mater.*, 2011, **23**, 2367-2371.

(23). (a) K. Hasan, A. K. Bansal, I. D. W. Samuel, C. Roldán-Carmona, H. J. Bolink and E. Zysman-Colman, *Scientific Reports*, 2015, **5**, 12325; (b) For examples see: S. Ladouceur, D. Fortin and E. Zysman-Colman, *Inorg. Chem.*, 2011, **50**, 11514-11526.

(24). M. S. Lowry, W. R. Hudson, R. A. Pascal Jr. and S. Bernhard, *J. Am. Chem. Soc.*, 2004, **126**, 14129-14135.

(25). S. Ladouceur, D. Fortin and E. Zysman-Colman, *Inorg. Chem.*, 2010, **49**, 5625-5641.

(26). H. Ishida, S. Tobita, Y. Hasegawa, R. Katoh and K. Nozaki, *Coord. Chem. Rev.*, 2010, **254**, 2449-2458.

(27). (a) J. V. Caspar and T. J. Meyer, *J. Phys. Chem.*, 1983, **87**, 952-957; (b) M. Bixon, J. Jortner, J. Cortes, H. Heitele and M. E. Michel-Beyerle, *J. Phys. Chem.*, 1994, **98**, 7289-7299.

(28). R. D. Costa, E. Ortì, H. J. Bolink, S. Graber, S. Schaffner, M. Neuburger, C. E. Housecroft and E. C. Constable, *Adv. Funct. Mater.*, 2009, **19**, 3456-3463.

(29). D. Tordera, S. Meier, M. Lenes, R. D. Costa, E. Ortí, W. Sarfert and H. J. Bolink, *Adv. Mater.*, 2012, **24**, 897-900.

(30). M. Lenes, G. Garcia-Belmonte, D. Tordera, A. Pertegás, J. Bisquert and H. J. Bolink, *Adv. Funct. Mater.*, 2011, **21**, 1581-1586.

(31). For representative of white-emitting LEECs see: L. He, J. Qiao, L. Duan, G. Dong, D. Zhang, L. Wang and Y. Qiu, *Adv. Funct. Mater.*, WILEY-VCH Verlag, 2009, **19**, 2950-2960.

(32). A. Deb, S. Manna, A. Maji, U. Dutta and D. Maiti, *Eur. J. Org. Chem.*, 2013, **2013**, 5251-5256.

(33). A. L. Kanibolotsky, R. Berridge, P. J. Skabara, I. F. Perepichka, D. D. C. Bradley and M. Koeberg, *J. Am. Chem. Soc.*, 2004, **126**, 13695-13702.

TOC

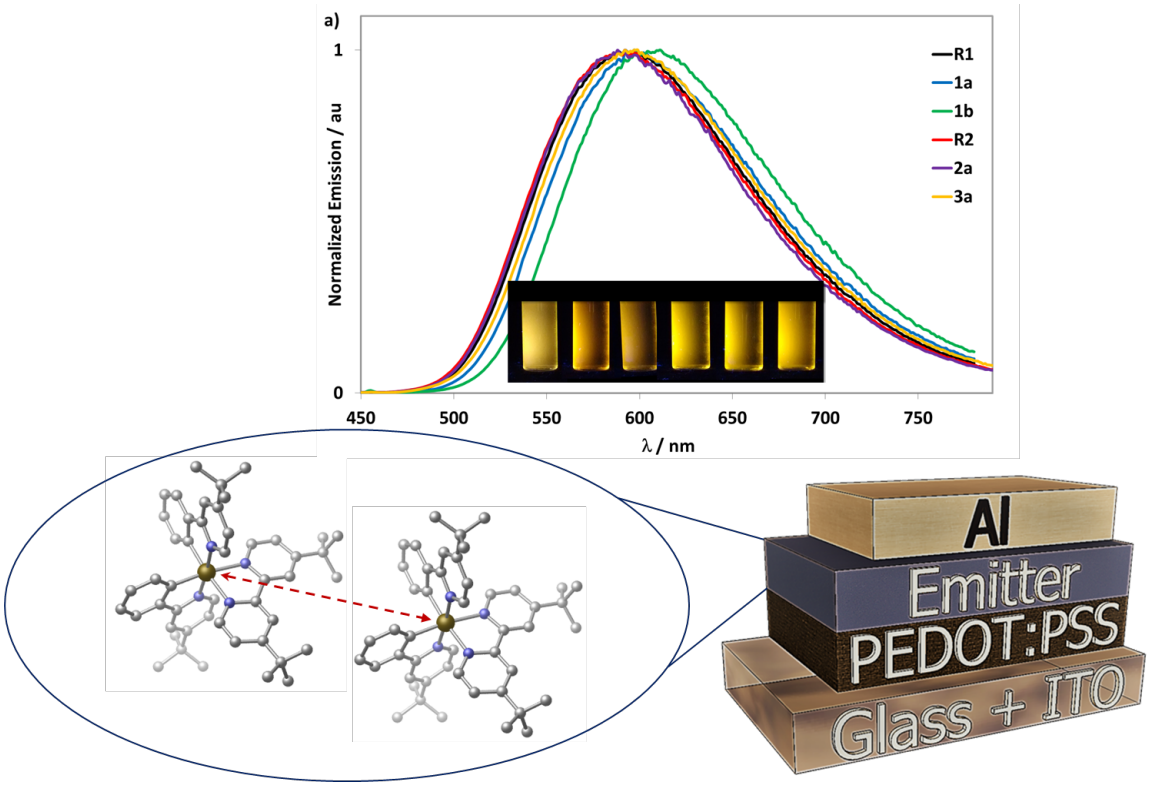
a)
1
0
Normalized Emission / au
450
500
550
600
650
700
750
λ / nm
R1
1a
1b
R2
2a
3a
Al
Emitter
PEDOT:PSS
Glass + ITO